Computers and Structures 240 (2020) 106335

Contents lists available at ScienceDirect

Computers and Structures

journal homepage: www.elsevier.com/locate/compstruc

Graphic statics in a continuum: Strut-and-tie models for reinforced concrete

Salma Mozaffari [a,*], Masoud Akbarzadeh [b], Thomas Vogel [a]

[a] Institute of Structural Engineering, ETH Zurich, Switzerland
[b] Polyhedral Structures Laboratory, Weitzman School of Design, University of Pennsylvania, Philadelphia, USA

ARTICLE INFO

Article history:
Received 12 March 2020
Accepted 9 July 2020
Available online 6 August 2020

Keywords:
Strut-and-tie model
Graphic statics
Layout optimization
Load path optimization
Reinforced concrete

ABSTRACT

This research bridges the gap between the numerical layout optimization method and the geometry-based analysis and design method of graphic statics. The study connects the two methods for the application of strut-and-tie models in reinforced concrete design. It suggests a new algorithm for the algebraic graphic statics of indeterminate trusses inspired by the layout optimization method. This research also contributes to the field of graphic statics by providing a formulation that generates form and force diagrams in a continuum, where the topology for none of the diagrams is initially provided.

The generation of strut-and-tie models for reinforced concrete has extensively relied on optimization methods, which are helpful techniques for the initiation of a load path inside a continuous domain. However, the resulting truss model is a single answer, and there exists limited control to methodically modify the topology or the force distribution of the model. Furthermore, the minimized-weight truss does not guarantee a practical strut-and-tie model or an optimized performance of a reinforcement design.

In contrast to the conventional optimization techniques with a single solution, the intuitive method of graphic statics provides the designer with a vast design space. It also offers explicit control over the geometry and force distribution of the generated truss models. The algorithm provided in this paper is applied to various continuous domains to systematically generate a variety of strut-and-tie models, their force diagrams, and constant stress fields. The production of the optimized truss model and its force distribution allows the direct interactive manipulations of the design while observing the changes in the stress fields and the reinforcement arrangement. The open-source repository of the implemented integrated algorithm and the examples used in this paper are also provided.

1. Introduction

The *truss model*, also known as *strut-and-tie model* (STM), is a set of compressive struts and tensile ties, which represents the load transfer mechanism in a reinforced concrete member [1,2]. The model has been intuitively developed to understand the behavior of cracked reinforced concrete, where concrete only contributes to the compression and steel is activated in tension [3,4]. The concept has later found justification in the lower bound theorem of plasticity [5–7]. Thus, the method results in conservative solutions [8]. A combination of STM with stress fields is typically used in practice to provide safe solutions. STM and stress fields are complementary in satisfying equilibrium and yield criteria of the lower bound theorem of plasticity [7,9].

The strut-and-tie method has a tremendous educational advantage over the *finite element analysis* (FEA) methods as it simplifies the understanding of bending and shear transfer inside a concrete element, thus it aids in a simplified calculation of required reinforcement quantity and location. Its combination with stress fields can also assure the capability of concrete to handle compressive stresses. Other than educational value, the method is used in practice and is introduced in concrete design guidelines [10–13] for both structural design and analysis [7,14]. Although the conventional FEA methods can provide more advanced analysis with refined material models, it is more of an analysis approach than a design tool. FEA rather focuses on assessing the input problem than providing the freedom to decide on the flow and arrangement of the tensile and compressive forces, which could dictate various structural behaviors. With this in mind, truss models and FEA

* Corresponding author.
E-mail addresses: mozaffari@ibk.baug.ethz.ch (S. Mozaffari), masouda@upenn.edu (M. Akbarzadeh), vogel@ibk.baug.ethz.ch (T. Vogel).

https://doi.org/10.1016/j.compstruc.2020.106335
0045-7949/

could also be used in parallel to assure a sound design, as we will demonstrate in the example of Section 3.3.

1.1. Generating a strut-and-tie model

Initially, STM is created intuitively and iteratively, similar to the *load path method* introduced by Schlaich et al. [8]. Later, various formulations of FEA method were employed, where the model is formed by aligning the struts and ties according to the direction of principal stresses (Fig. 1(a) and (b)) [8,14,15]. Other than getting help from FEA, STMs were generated using other methods such as *topology optimization* (TOPOPT) (Fig. 1(c) and (d)) [16–19] and *layout optimization* (LAYOPT) also known as *ground truss optimization*, and *discrete/truss topology optimization* (Fig. 1(e) and (f)) [20–22].

TOPOPT and LAYOPT minimize the material distribution in continuous and discrete design domains, respectively, where the concentration of the material as the result of the optimization is on the path of higher stresses. Similar to principal stresses from FEA, the output material pattern of TOPOPT could hint on manual conceiving of a truss model. Further analysis is also needed to calculate the internal forces of the STM. On the other hand, the solution of LAYOPT is the truss member forces, where the non-zero forces result in an in-equilibrium truss model. Therefore, the use of LAYOPT to initiate an STM is automatic and requires fewer steps.

1.2. Problem statement

All the mentioned techniques help in initiating and understanding of a load transfer mechanism inside a given domain accounting for the boundary conditions. However, the resulting trusses can include impractical tension–compression arrangements for the design using STM. The attention has typically given to more elaborate formulations or more realistic material models [14,15,19,21,22,24–27]. The examples of Fig. 1 show how the devised truss models have impractical diagonal reinforcements.

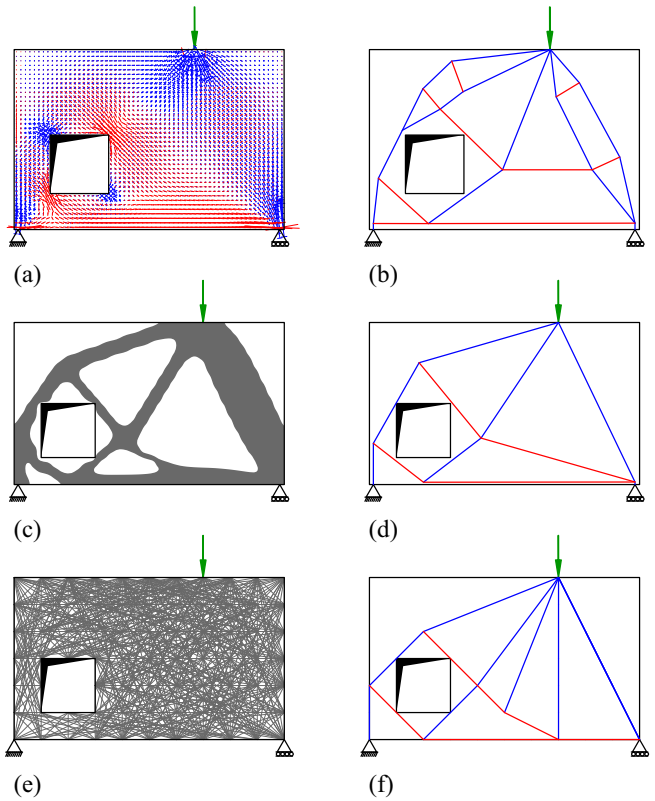

Fig. 1. (a) Principal stresses from FEA; (b) devised STM based on the direction of principal stresses in (a); (c) material distribution pattern from TOPOPT [23]; (d) devised STM from (c); (e) ground truss for LAYOPT; (f) non-zero-force truss memb. ers from LAYOPT.

A valid STM usually follows structural engineering conventions and seeks more facile reinforcement fabrication. So, it requires proper reinforcement inclination (i.e., typically horizontal or vertical) and location, acceptable angles between struts and ties (i.e., more than 25 degrees according to the guidelines), and no overlapping tension–compression members [8,12]. One could modify the FEA/optimization equations by embedding the rules for achieving a valid STM, although depending on the formulation, the process could turn out as counter-intuitive. In the end, optimization methods produce a single solution for the minimized-weight truss, which does not guarantee an optimized performance of a reinforcement design. Furthermore, these methods provide the designer with limited control to modify the output topology and its force distribution to generate multiple valid solutions and hence, varied structural performances.

1.2.1. The STM and the geometry-based design methods

The geometry-based method of *graphic statics* (GS) was applied in the literature while creating STMs for reinforced concrete elements [7,28–30]. This method's application had various reasons such as assuring the equilibrium of forces, controlling the magnitude of the internal truss forces, and creating multiple STM solutions for a given problem.

The method of GS is a potent design technique that has been practiced and researched by many structural designers and researchers since the early nineteenth century [31–41]. Graphic statics provides explicit control over the truss's geometry and its internal force magnitudes within the same state of global/external equilibrium. The availability of the force in a geometric setting provides the opportunity: (i) to create a variety of solutions through manipulation or subdivision of the force diagram [42–46]. (ii) to optimize trusses using load path minimization algorithms [38,47]. (iii) to create constant stress fields using the geometrical summation (*Minkowski sum*) of the form and force diagrams [48–51].

1.2.2. Graphic statics in a continuous field

Even though GS provides the freedom to modify the form or force diagrams while maintaining the equilibrium conditions, it requires the definition of a starting topology for the form or force diagram, where the materialization of the form typically happens in the next step. So, the extraction of a load path for a given materialized domain, such as a reinforced concrete block, under specified boundary conditions using GS requires interactive procedures or a manual definition of a starting geometry [7,28,29,47]. Furthermore, the algebraic formulations of GS [52–54] generate the dual diagram (force or form) automatically, but still needs the input for the primal diagram (form or force).

1.2.3. Summarizing the limitations of current techniques

To sum up, several techniques such as GS, FEA, TOPOPT, and LAYOPT have been used and helped in creating strut-and-tie models. Although the method of GS is promising in generating multiple solutions and assuring the equilibrium, it requires a starting geometry for one of the form or force diagrams. In contrast, the optimization or FEA methods help in initiating and understanding of a load transfer mechanism. However, they have a black-box nature, and they provide the designer with limited control to modify the output topology or its force distribution. Besides, their formulations require modifications to result in practical truss models.

This study aims to utilize the optimization methods' strengths in the automatic generation of a valid model. So, the drawback of GS in requiring a pre-defined form or force diagram is avoided. LAYOPT is selected since, as mentioned, it requires fewer steps to

generate a truss. Furthermore, the goal is to engage GS as a highly capable technique to help create a design space, where the designer could alter the truss geometry and its member forces. Thus, the disadvantage of optimization in providing a single solution is avoided.

1.3. Objectives and contributions

The objective of this research is to bridge the gap between LAYOPT and GS by utilizing their advantages. Therefore, as a contribution to the field of graphic statics, the algorithm of this paper can be used to generate form and force diagrams for a continuum under specified boundary conditions, where the topology for none of the diagrams is initially provided. Furthermore, contrary to the conventional optimization techniques with a single solution, the availability of the form and force diagrams facilitates further modifications and improvements of the initial solutions.

The novel algorithm implements the *algebraic graphic statics* (AGS) of an indeterminate truss inspired by the LAYOPT technique. Therefore, there is no requirement for pre-assigning force densities to specified members of an indeterminate form diagram. This paper extends the scope of the previous research of the authors presented in [50] on the integration of *algebraic graphic statics* (AGS) into a LAYOPT algorithm by providing a detailed explanation of the methods, their limitations, and the combination of the form and force diagrams using the Minkowski sum operation to produce stress fields.

The paper then takes the research to a further stage, where with the help of GS, the manipulation of the produced geometry with an immediate update of the internal forces is feasible. The generation of the optimized truss model and its force distribution allows the interactive modifications, where the changes in the stress fields and the reinforcement arrangement are observable. As a result, multiple valid STM/stress field solutions and reinforcement designs could be produced.

1.4. Paper outline and nomenclatures

Section 2 provides the theoretical background for the study in the following order: the definition of ground truss and the equations of LAYOPT (Section 2.1); the properties of form and force diagrams and algebraic formulation of GS (Section 2.2); an integration of LAYOPT, AGS, and Minkowski sum operation into a computational set-up to initiate an STM, its force diagram, and constant stress fields (Section 2.3); and a method to modify the initially generated diagrams using GS (Section 2.4). Section 3 shows the implementation of the integrated algorithm on several boundary conditions, where in the next step, GS helps modify the initial solutions, and Section 4 concludes the paper with an outlook to the further steps of the research.

Table 1 presents the notations used in this paper. Matrices and vectors are denoted by bold uppercase and lowercase letters, respectively. The topological information of the form and force diagrams are represented with italic letters and italic letters with an asterisk (*) sign, respectively.

In all figures, except Fig. 14, the red color shows tension, and the blue color displays compression forces/stresses. In Fig. 14(3), red shows compression and blue tension.

Table 1
Nomenclature for the notations used in this paper and their corresponding descriptions.

Topology	*Description*
Γ	primal/form diagram
Γ^*	dual/force diagram
S	Minkowski sum of Γ and Γ^* (constant stress fields)
R	reinforcement layout
v_{gt}	# of vertices of ground truss
e_{gt}	# of edges of ground truss
v	# of vertices of Γ
v_{int}	# of internal vertices of Γ
e	# of edges of Γ,
f	# of faces of Γ
v^*	# of vertices of Γ^*, $v^* = f$
e^*	# of edges of Γ^*, $e^* = e$
f^*	# of faces of Γ^*, $f^* = v_{int}$
Matrices	
$\mathbf{C}^*$	vertex-edge incidence matrix of Γ^*
$\mathbf{A}_{opt}$	equilibrium matrix of LAYOPT
$\mathbf{A}_{ags}$	equilibrium matrix of AGS
$\mathbf{A}_d, \mathbf{A}_{id}$	partitions of $\mathbf{A}_{ags}$
$\bar{\mathbf{A}}_{ags}$	reduced-row $\mathbf{A}_{ags}$
$\bar{\bar{\mathbf{A}}}_{ags}$	reduced-row-column $\mathbf{A}_{ags}$
$\mathbf{Q}$	diagonal matrix of $\mathbf{q}$
$\mathbf{L}^*$	Laplacian of $\mathbf{C}^*$
$\bar{\mathbf{B}}$	face-edge matrix of Γ
$\mathbf{B}$	face-edge matrix of Γ with additional rows
$\mathbf{I}$	identity matrix
Vectors	
$\mathbf{u}$	x-coord differences of v
$\mathbf{v}$	y-coord differences of v
$\mathbf{x}^*$	x-coords of v^*
$\mathbf{y}^*$	y-coords of v^*
$\mathbf{q}$	solution of the AGS equilibrium equation
$\mathbf{q}_d, \mathbf{q}_{id}$	partitions of $\mathbf{q}$
$\bar{\mathbf{q}}_{id}$	force density of the ground truss members
$\bar{\mathbf{q}}_{id,diag}$	force density of the ground truss diagonal members
$\mathbf{l}$	length of the ground truss members
$\mathbf{l}_e$	edge lengths of the reconstructed Γ
$\mathbf{a}$	cross-sectional area of the ground truss members
$\mathbf{b}$	assigned edge lengths
$\boldsymbol{\omega}$	vector of ones
$\mathbf{f}_{gt}$	force magnitude of the ground truss members
$\mathbf{f}_{gt,diag}$	force magnitude of the diagonal ground truss members
$\mathbf{f}$	external loads
$\mathbf{f}_r$	external loads and support reactions
Parameters	
σ_C	factored concrete yield stress in compression
σ_T	factored steel yield stress in tension
Other	
V	total volume of the structure
n_r	# of support reactions
k	# of independent densities (lenght of $\mathbf{q}_{id}$)
b	width of stress field
t	thickness of concrete element
α	scale factor for Minkoswki sum
γ	scale factor for Γ^*
Φ	required reinforcement

2. Methodology

The flowchart of Fig. 2 illustrates the research methodology. The main goal of this section is to engage GS in the automatic process of generating STM solutions and their force diagrams without the need to pre-define the form diagram. We explain the equations of LAYOPT, the properties of the reciprocal diagrams, and the algebraic formulation of graphic statics. The implementations of LAYOPT, AGS as well as the Minkowski sum operation will then be integrated into a single computational set up to initiate a valid truss model, its force diagram, and constant stress fields. In Sections 2.4 and 3.2, we use the generated form and force diagrams to manipulate the STM geometry and its force distribution to create other valid solutions and reinforcement designs.

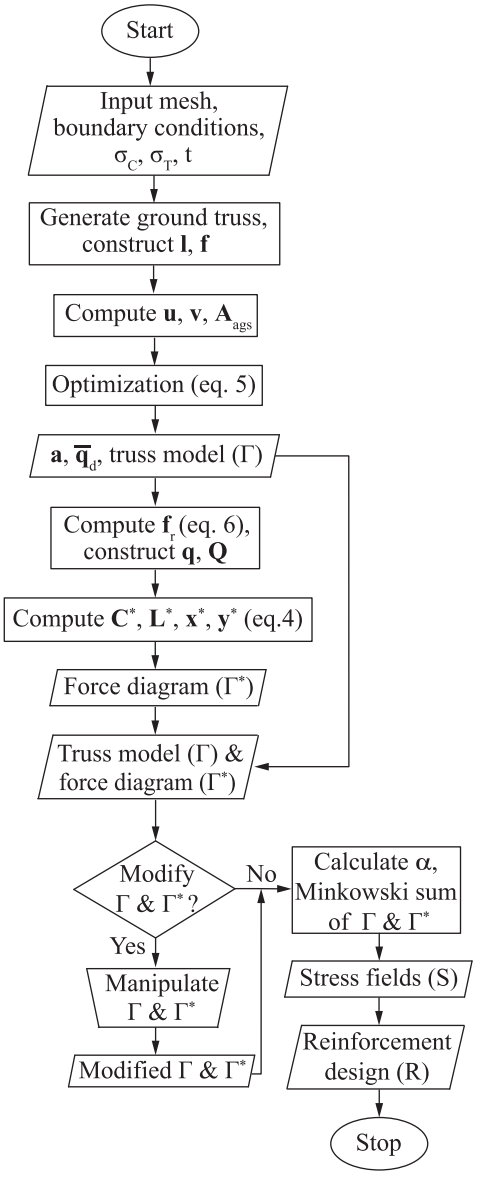

Fig. 2. Flowchart of the research methodology.

2.1. Layout optimization

In Section 1.1, we discussed that using LAYOPT helps in the automatic generation of a truss model and therefore requires fewer steps compared to using TOPOPT or FEA. In this section, we apply the plastic formulation of LAYOPT, which is based on equilibrium and not compatibility or stress–strain relations [55]. The linear nature, i.e., linear force-stress relationship, of this formulation allows the objective function to either aim for a volume or a load path minimization, which theoretically yields the same output [56]. The total load path of the truss is obtained by the summation of each truss member's internal force multiplied by its length. The minimization of the load path is a common objective while utilizing GS methods [38,47]. Although in this paper, the input geometry (i.e., a ground truss) is created automatically, the equations are linear, and the location of the nodes stay unchanged.

The starting geometry for LAYOPT is a ground truss. The ground truss is defined in two common ways; first-order and full ground truss (e.g., Fig. 3(a) and (b)). For a ground truss with e_{gt} members (edges), v_{gt} nodes (vertices), and n_r support reactions, the plastic formulation is given as

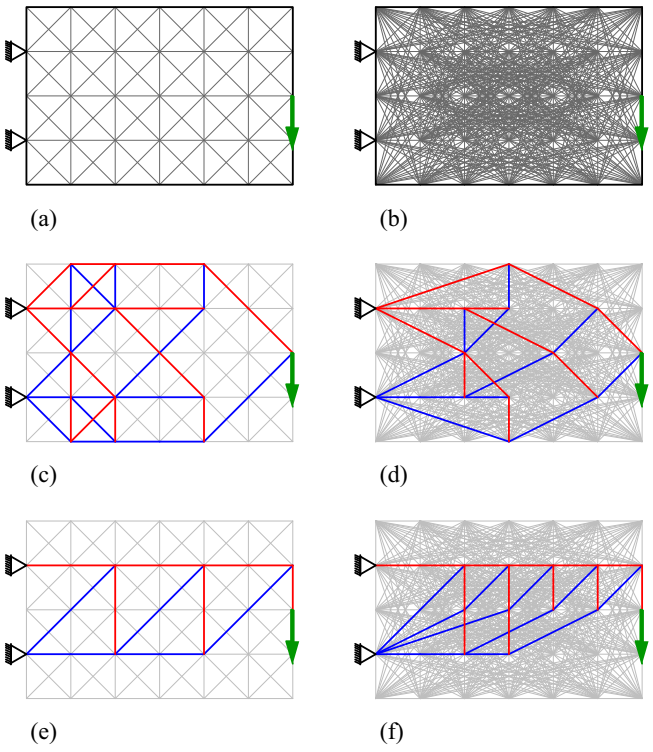

Fig. 3. (a) First-order ground truss; (b) full ground truss; (c) and (d) optimum layouts for (a) and (b); (e) and (f) optimum layouts for (a) and (b) with the additional constraint in (1e) (zero or minimal forces in (c)-(f) are. in light gray).

$$\min_{\mathbf{a},\mathbf{f}_{gt}} \quad V = \mathbf{l}^T\mathbf{a} \tag{1a}$$

$$\text{s.t.} \quad \mathbf{A}_{opt}\mathbf{f}_{gt} = \mathbf{f} \tag{1b}$$

$$-\sigma_C\mathbf{a} \leqslant \mathbf{f}_{gt} \odot \boldsymbol{l} \leqslant \sigma_T\mathbf{a} \tag{1c}$$

$$\mathbf{a} \geqslant \mathbf{0} \tag{1d}$$

$$\mathbf{f}_{gt,diag} \leqslant \mathbf{0} \tag{1e}$$

where V is a scalar for total volume of the structure, $\mathbf{l}^\mathbf{T}$ $[1 \times e_{gt}]$ and $\mathbf{a}$ $[e_{gt} \times 1]$ are the vectors of length and cross-sectional area of the ground truss members. The objective in (1a) is to minimize the total volume subjected to three constraints: (1b) the equilibrium constraint with $\mathbf{A}_{opt}$ the $[(2v_{gt} - n_r) \times e_{gt}]$ the equilibrium matrix built from directional cosines of the members, $\mathbf{f}_{gt}$ the $[e_{gt} \times 1]$ member forces vector and $\mathbf{f}$ the external loads vector. (1c) the stress constraint with σ_C and σ_T as factored yield stresses in compression (concrete) and tension (steel). (1d) the limitation of the areas to non-negative values. (1e) the limitation of force magnitudes in the diagonal members, $\mathbf{f}_{gt,diag}$, to non-positive values (i.e., defined as either compressive or zero forces).

The optimization outputs (design variables) are the ground truss member forces, $\mathbf{f}_{gt}$, and cross-sectional areas, $\mathbf{a}$. Members with zero or minimal cross-sectional areas, i.e., also with zero or minimal forces, will be removed, leading to a truss topology as a subset of the ground truss. Fig. 3(c) and (d) show the results of the original LAYOPT formulation, i.e., with the constraints (1b)-(1d), and Fig. 3(e) and (f) show the solutions with all constraints. The additional constraint in (1e) makes the reinforcement directions more practical. The results of Fig. 3 illustrate their dependency on the ground truss definition. To avoid overlapping tension–compression members and to have a model with practical reinforcement layouts, we decided to use the first-order ground truss and the constraints (1b)-(1e) as a base to initiate an STM.

2.2. Graphic Statics

In this section, we explain the concept of reciprocal diagrams and the algebraic formulation of GS. Using GS offers explicit control over the geometry of a truss and its internal force magnitudes within the same state of external equilibrium. Although, applying this method in generating multiple STM solutions requires a starting geometry that accounts for the design domain constraints and boundary conditions. In the next section, we use the optimized truss geometry from the LAYOPT algorithm as the starting geometry for GS.

GS's form and force diagrams represent the geometry of a truss-like structure and the force magnitudes of its members, respectively. The reciprocity between the two diagrams assures global and nodal equilibrium and provides access to the member force magnitudes and support reactions. Fig. 4(a) and (b) show an example of a truss or form diagram, Γ, and its corresponding force diagram, Γ^*. The length of each edge e_i^* in Γ^* is proportional to the force magnitude in its reciprocal edge e_i in Γ. For each nodal force equilibrium in Γ, there exists a closed force polygon in Γ^* (Fig. 4(d) and (e)). The global equilibrium between the external loads and support reactions is also a closed force polygon in Γ^* (Fig. 4(c)). For example, the polygon surrounding the f_i^* face in Fig. 4(b) shows the equilibrium of forces at node v_i in Fig. 4(a). Similarly, each node v_i^* in Γ^* has a reciprocal face f_i in Γ. Note that the lengths of the edges in Γ^* are proportional to the force magnitudes, and the force diagram scale, γ, is calculated, for instance, by finding the ratio of the $\mathbf{f_j}$ external force magnitude, to its reciprocal edge length, $l_{e_j^*}$.

As a result of reciprocity, the number of truss nodes, v_{int}, of Γ are equal to the number of faces in Γ^*, which is equivalent to the number of closed polygons (loops) in Fig. 4(d) and (e). Also, the number of edges of Γ and Γ^* are equal. The load and support reactions in Γ count as edges. The edges of Γ^* count as the four green edges in Fig. 4 and non-repetitive blue and red edges in Fig. 4(d) and (e). Finally, the number of faces of Γ is the same as the number of vertices of Γ^*. The faces count as four internal faces and three virtual faces between the load and support locations.

2.2.1. Algebraic Graphic Statics

The algebraic formulation of graphic statics is a non-procedural approach to generate the force diagram given a form. As the method is fully explained in [52], the focus here is limited to the fundamental equations and concepts.

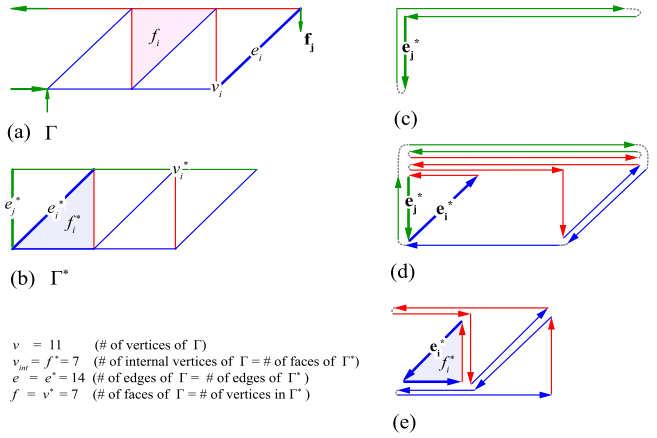

Fig. 4. (a) Form diagram, Γ; (b) force diagram, Γ^*; (c) global force polygon (external equilibrium); (d) force polygons of the boundary nodes (equilibrium at the nodes connected to external load/support reactions); (e) force polygons of the internal nodes.

For a form diagram with e edges (including the edges related to the external loads and supports), v vertices, and v_{int} internal vertices (excluding the leaf vertices), the equilibrium equation follows

$$\mathbf{A}_{ags}\mathbf{q} = \mathbf{0} \tag{2}$$

where $\mathbf{A}_{ags}$ is the $[2v_{int} \times e]$ equilibrium matrix and $\mathbf{q}$ is the $[e \times 1]$ vector of force densities. Force density is the ratio of the member force to its length. This equation is similar to the equilibrium constraint in (1b). The differences are: (i) instead of the member forces vector $\mathbf{f}_{gt}$, force densities vector $\mathbf{q}$ is used. (ii) the right side of the equation is a null vector since $\mathbf{q}$ includes the density of the leaf edges, i.e., the edges related to external loads and support reactions with arbitrary lengths, and $\mathbf{A}_{ags}$ has the geometric information of the leaf edges. (iii) instead of the directional cosines of the members, $\mathbf{A}_{ags}$ only includes the directional coordinate differences (the division by the member length is compensated in the force densities vector $\mathbf{q}$).

The unknown or dependent partition of $\mathbf{q}, \mathbf{q}_d$ $[(e-k) \times 1]$, if $\mathbf{A}_d$ is square and non-singular, is calculated as

$$\mathbf{q_d} = -\mathbf{A}_d^{-1}\mathbf{A}_{id}\mathbf{q}_{id} \tag{3}$$

where $\mathbf{q}_{id}$ $[k \times 1]$ is the vector of given or independent densities, which can be assumed as the density of external loads, and $\mathbf{A}_d$ $[2v_{int} \times (e-k)]$ and $\mathbf{A}_{id}$ $[2v_{int} \times k]$ are the partitions of $\mathbf{A}_{ags}$. Since $\mathbf{A}_d$ is considered a square matrix, $2v_{int} = (e-k)$.

By reconstruction of $\mathbf{q}$ after the calculation of $\mathbf{q}_d$ from (3), the coordinates of the force diagram are obtained as

$$\begin{aligned} \mathbf{x}^* &= \mathbf{L}^{*^{-1}}\mathbf{C}^*\mathbf{Q}\mathbf{u} \\ \mathbf{y}^* &= \mathbf{L}^{*^{-1}}\mathbf{C}^*\mathbf{Q}\mathbf{v} \end{aligned} \tag{4}$$

where $\mathbf{x}^*$ and $\mathbf{y}^*$ $[v^* \times 1]$ are the vertex coordinates of the force diagram, $\mathbf{C}^*$ $[v^* \times e]$ is the vertex-edge incidence matrix representing the topology of the force diagram, $\mathbf{Q}$ $[e \times e]$ is the diagonal matrix of vector $\mathbf{q}, \mathbf{u}$ and $\mathbf{v}$ $[e \times 1]$ are the coordinate differences of the form diagram, and $\mathbf{L}^* = \mathbf{C}^*\mathbf{C}^{*T}$ is the $[v^* \times v^*]$ Laplacian of $\mathbf{C}^*$. $\mathbf{C}^*, \mathbf{u}$, and $\mathbf{v}$ are known, once the geometry of the truss (e.g., Fig. 4(a)) is given. Having $\mathbf{y}^*, \mathbf{x}^*$, and $\mathbf{C}^*$, one can plot the force diagram (e.g., Fig. 4(b)).

2.2.2. Limitations of the algebraic formulation

There are some limitations/challenges regarding the AGS method:

(i) In the case of indeterminate forms, the given or independent densities, $\mathbf{q}_{id}$, cannot only be assumed as the densities of the external load edges. The independent edges are selected based on the non-pivot columns of the *reduced row-echelon form* of $\mathbf{A}_{ags}$ [52]. Therefore, there exist several solutions, based on what one selects as the densities for those edges. For example, in the case of multiple external loads, if the edges related to the external loads are not a part of independent edges, then, to maintain the external load values as fixed magnitudes, it is not always trivial to find the correct combination of independent edges.

(ii) To define the incidence matrix $\mathbf{C}^*$ representing the topology of force diagram (i.e., the dual graph), the geometry of the form needs to be a planar straight-line graph with no overlapping spaces. The algorithms of creating a planar graph are complicated and not always result in a useful form [52].

(iii) AGS still requires the definition of a starting geometry, which considers the boundary conditions and geometrical constraints of the design domain.

2.3. Integrated algorithm

Section 1.3 mentioned that the aim is to overcome the drawbacks of optimization techniques and the GS method by integrating the advantages of LAYOPT and GS. In this section, we combine the formulations of LAYOPT and AGS for the automatic creation of a truss model and its force diagram. The AGS equilibrium matrix is modified and used along with the force densities as the new design variable in LAYOPT equations. The immediate advantage is that the output force densities can be directly used in (4) to generate the force diagram. Section 2.4 shows how the primary reciprocal diagrams will be then modified to construct other STM solutions.

Similar to LAYOPT, the integrated algorithm avoids a manual initiation of a starting topology [38,47] by generating the ground truss automatically. Also, since the optimization runs regardless of the indeterminacy of the starting or resulting truss, the AGS disadvantage of requiring the pre-assignment of independent force densities is removed. Furthermore, to avoid having issues, while constructing $\mathbf{C}^*$, with the non-planar first-order ground truss, a node is introduced at the intersection of the ground truss crossed members. The modified optimization formulation is given as

$$\begin{aligned} \min_{\mathbf{a},\bar{\mathbf{q}}_d} \quad & V = \mathbf{l}^T\mathbf{a} \\ \text{s.t.} \quad & \bar{\bar{\mathbf{A}}}_{ags}\bar{\mathbf{q}}_d = \mathbf{f} \\ & -\sigma_C\mathbf{a} \leqslant \bar{\mathbf{q}}_d \odot \boldsymbol{l} \leqslant \sigma_T\mathbf{a} \\ & \mathbf{a} \geqslant \mathbf{0} \\ & \bar{\mathbf{q}}_{d,diag} \leqslant \mathbf{0} \end{aligned} \tag{5}$$

where $\bar{\bar{\mathbf{A}}}_{ags}$ is a $[(2v_{gt} - n_r) \times e_{gt}]$ modified $\mathbf{A}_{ags}$ matrix, where the rows related to the support reactions and the columns corresponding to external loads and support edges are removed. $\bar{\mathbf{q}}_d$ $[e_{gt} \times 1]$ is the vector of force density for the ground truss members, $\bar{\mathbf{q}}_d \odot l$ is the element-wise product of the force density and length vectors, and $\bar{\mathbf{q}}_{d,diag}$ is a subset of $\bar{\mathbf{q}}_d$. Note that here v_{gt} is equivalent to v_{int} and e_{gt} to $e - (k + n_r)$. The design variables are $\bar{\mathbf{q}}_d$ and $\mathbf{a}$.

The vector $\bar{\mathbf{q}}_d$ from the optimization in (5) is used to construct the complete force density vector $\mathbf{q}$, which includes densities of the external loads and support reactions. The support reactions can be calculated as

$$\mathbf{f}_r = \bar{\mathbf{A}}_{ags}\bar{\mathbf{q}}_d \tag{6}$$

where the non-zero elements of $\mathbf{f}_r$ $[2v_{gt} \times 1]$ are the external loads and the support reactions, and $\bar{\mathbf{A}}_{ags}$ is a $[2v_{gt} \times e_{gt}]$ modified $\mathbf{A}_{ags}$ matrix, where the columns corresponding to external loads and support edges are removed. The diagonal matrix of $\mathbf{q}$, $\mathbf{Q}$, along with the generated $\mathbf{C}^*$, $\mathbf{u}$, and $\mathbf{v}$ of the output truss is then used in (4) to calculate the coordinates of the force diagram.

2.3.1. Stress fields

The availability of the form and force diagrams allows the creation of constant stress fields using the Minkowski sum operation [48–50]. Assume vertex v_i, its connecting edges, e_i, e_j, and e_k, and their rotated reciprocal vectors, $\mathbf{e}_i^*, \mathbf{e}_j^*$, and $\mathbf{e}_k^*$ in Fig. 5(a) and (b). Minkowski sum of e_i and $\boldsymbol{\alpha}\mathbf{e}_i^*$ is illustrated as the resulting rectangular area from offsetting edge e_i in the direction of vector $\boldsymbol{\alpha}\mathbf{e}_i^*$ from v_0 in Fig. 5(c). The same procedure follows for e_k with $\boldsymbol{\alpha}\mathbf{e}_k^*$ from point v_1, then, for e_j with $\boldsymbol{\alpha}\mathbf{e}_j^*$ from point v_2. The resulting rectangular areas along truss bars and the polygon at the nodal region (Fig. 5(c)) are similar to constant stress fields with *hydro-static* nodes (i.e. the geometry of each node is obtained using the constant factored yield compressive strength σ_C) [9,57]. Fig. 5(d) is formed by following the same procedure for other vertices and their connecting edges. Note that Fig. 5(d) is not immediately usable as stress fields since the compression fields overlap at some nodes. Therefore, adjustments required to make the stress fields valid by re-arranging the dual edges at the nodes (see Fig. 5(e)).

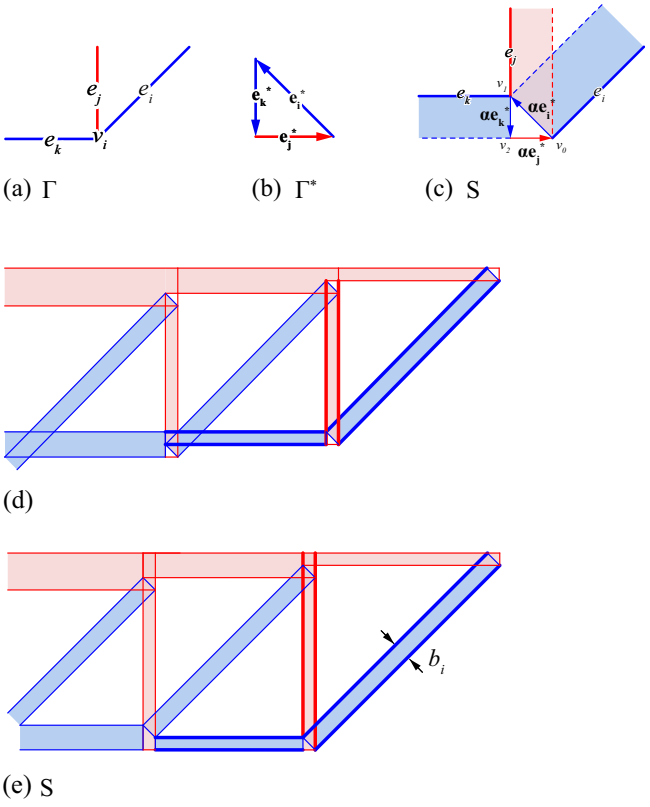

Fig. 5. (a) Node v_i and its connecting edges; (b) the rotated force (dual) polygon for node v_i; (c) Minkowski sum of the reciprocal edges in (a) and (b) with the scale factor α; (d) Minkowski sum for all the reciprocal edges in Fig. 4(a) and (b); (e) adjusted stress fields to avoid compression. field overlaps.

The width b_i of each stress field is defined in (7) and is related to the member force magnitude $\gamma l_{e_i^*}$, the thickness of the concrete element t, and the concrete factored yield compression stress σ_C. Therefore, the factor α in Fig. 5(c) is considered as $\frac{1}{\sigma_C t}$.

$$b_i = \frac{\gamma l_{e_i^*}}{\sigma_C t} \tag{7}$$

Fig. 6 show the three outputs of the integrated algorithm. In the examples of this paper, as a convention by structural engineers, the center lines of the tension fields are shown (Fig. 6(d)).

2.3.2. Effect of the mesh size

Before introducing a ground truss, the input design domain is discretized into simple square meshes. The decision on the mesh size of the defined domain is arbitrary, and the size could affect the resolution of the optimization solution by changing the connectivity pattern of the ground truss, for example, using a twice finer mesh than the mesh used in Fig. 6(a), does not change the solution in Fig. 6(f), although, in Fig. 7(e), the resulting truss with a finer mesh has more members compared to Fig. 7(b). Furthermore, in Fig. 7(e), the indirectness of the path between external load and supports causes a finer redistribution of the internal forces compared to Fig. 7(b), which is evident by comparing the force diagrams in Fig. 7(c) and (f).

Instead of playing with the mesh size to change the resolution of the STM solution, in Section 3.2, we show how, with the help of GS, the force and form diagrams can be subdivided to redistribute the forces systematically.

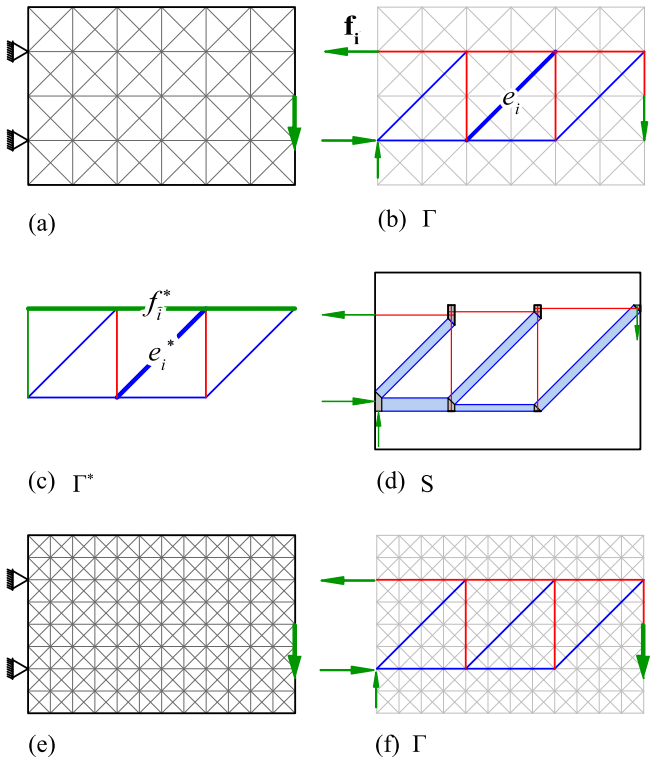

Fig. 6. (a) Input boundary conditions and ground truss; (b) output form diagram (STM); (c) output force diagram; (d) output stress fields; (e) input boundary conditions and ground truss with finer mesh; (f) output form diagram for (e).

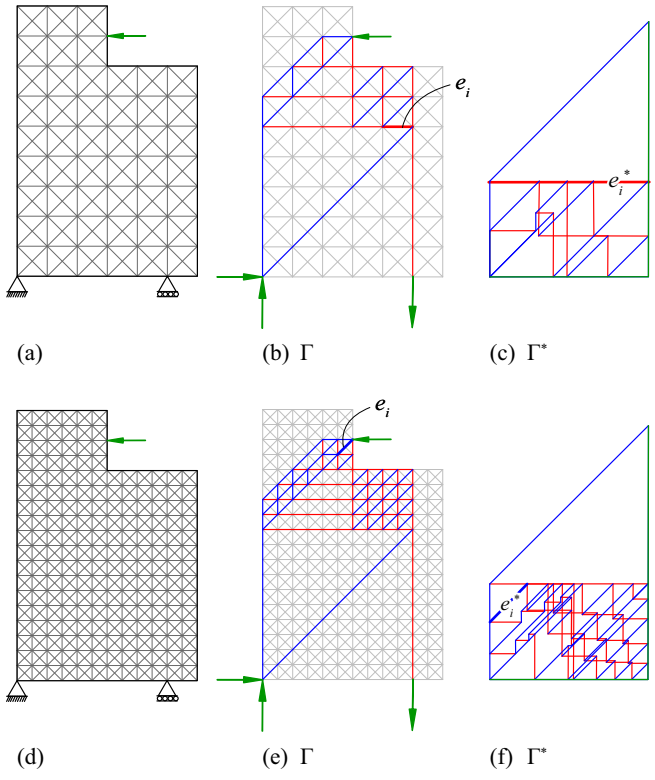

Fig. 7. (a) and (d) Boundary conditions and ground truss inputs; (b) and (e) output optimum forms (zero or minimal forces are in light gray); (c) and (f) output force diagrams.

2.4. Reconstruction of the STM from the modified force diagram

So far, the focus was on the implementation of the integrated algorithm, which runs the optimization in (5) to automatically create a valid truss model, then uses (4) to construct the force diagram, and lastly implements Minkowski sum to create stress fields. Now, that we have initiated a model and its force diagram, we can use the reciprocal relationships of GS to modify them. One way to modify the initial results is to change the force diagram and update the form subsequently. This way, one can assure the equilibrium by keeping the force polygons closed and control the magnitude of the forces. The updating of the form diagram after modifying the force diagram uses a different method than the *bi-directional graphic statics* introduced in [53], where only the nodal movements of the force diagram are addressed. To clarify the modification process, assume the outputs of the integrated algorithm in Fig. 8(b) and (c). Consider adding a stirrup on the left side of the truss. The steps of the modification process are as follows:

(i) Make a self-stressed network of the truss model by connecting the end vertices of the load edges, as in Fig. 8(d). That creates an extra face, $[v_4, v_5, v_6, v_7]$. These new "virtual" edges help in the reconstruction of the form in the last step.
(ii) Update the force diagram to include the forces of the virtual edges by running an AGS algorithm using equations (2), (3), and (4) as in Fig. 8(e). Fig. 8(f) shows the force polygons in the updated force diagram.
(iii) Apply changes to the force diagram, as in Fig. 8(g). This step could include removing/adding edges and vertices from/to the force diagram. One needs to make sure that the modified shape has closed force polygons.
(iv) Find the edge lengths of the new form diagram. In this step, we find the faces of the new form using the new closed force polygons. Around each face, we select a consistent orientation of the edges. Since each face provides a closed loop of edges, the sum of edge vectors has to be the zero vector. Each face provides two equations for the edge lengths, i.e., the summation of x and y coordinates of the edge vectors equals zero. This can be written in an algebraic format [58] as

$$\bar{\mathbf{B}}\mathbf{l}_e = \mathbf{0} \tag{8}$$

where $\bar{\mathbf{B}}$ is a $[2f \times e]$ matrix, that describes the geometry of the form graph, with f number of the faces in the new form diagram and e the total number of edges including the leaf and virtual edges. $\mathbf{l}_e$ $[e \times 1]$ is the vector of edge lengths of the new form diagram and the solution of (8).

To have a unique solution for (8), one requires to assign edge lengths to some of the unchanged edges. The number of edge lengths that can be assigned depends on the *geometric degrees of freedom* of the form [58]. The geometric degree of freedom is 3 for the unreconstructed form of this example. Since the virtual edges normally stay unchanged, here we assign the edge lengths for (v_6, v_7), (v_4, v_7), and (v_4, v_6). The unique solution for the edge lengths of the new form is

$$\mathbf{l}_e = \mathbf{B}^{+}\mathbf{b} + [\mathbf{I} - \mathbf{B}^{+}\mathbf{B}]\boldsymbol{\omega} \tag{9}$$

where matrix $\mathbf{B}$ $[(2f+3) \times e]$ has three additional rows compare to $\bar{\mathbf{B}}$. Each additional row represents one of the edges with an assigned edge length, which is a vector with zeros everywhere, except 1.0 at the location of that edge. $\mathbf{B}^{+}$ $[e \times (2f+3)]$ is the *Moore–Penrose inverse* of $\mathbf{B}$ [59,60]. $\mathbf{b}$ is a $[(2f+3) \times 1]$ vector of zeros, except in the last three elements, where it includes the edge lengths of the selected

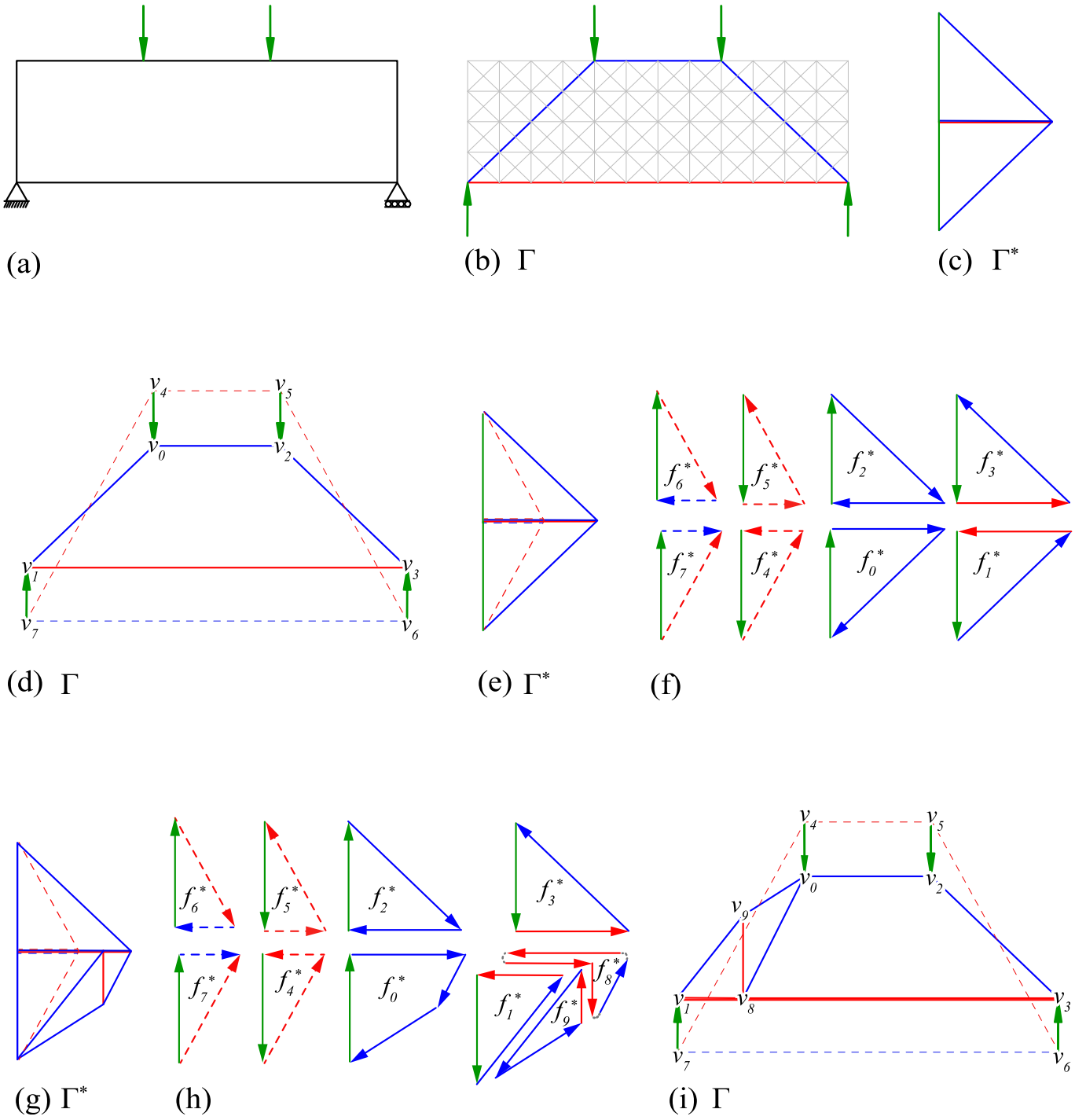

Fig. 8. (a) Input boundary conditions; (b) output truss model; (c) output force diagram; (d) self-stressed form; (e) force diagram for (d); (f) force polygons in (e); (g) modified force diagram; (h) force polygons in (g); (i) reconstructed form diagram.

edges. $\mathbf{I}$ is the $[e \times e]$ identity matrix and $\boldsymbol{\omega}$ is a $[e \times 1]$ vector of ones.

(v) Reconstruct the new form. Now that the edge lengths for the new form diagram are known, it can be reproduced. The reconstruction uses a basic *breadth-first search* algorithm [61]. It starts from a fixed nodal location like node v_4, then, finds the location of its neighboring nodes using the vector directions (i.e., edge orientations) picked while constructing the $\bar{\mathbf{B}}$ matrix and the edge lengths obtained from (9). The same procedure will follow for the neighbors of the neighboring nodes until all the nodes are covered. Fig. 8(i) shows the new solution for the truss model, the virtual edges can be removed from force and form diagrams, after the reconstruction.

2.5. Implementation

An open-source repository is generated to implement the integrated algorithm for the examples presented in this paper [62]. The computation time for the integrated algorithm is

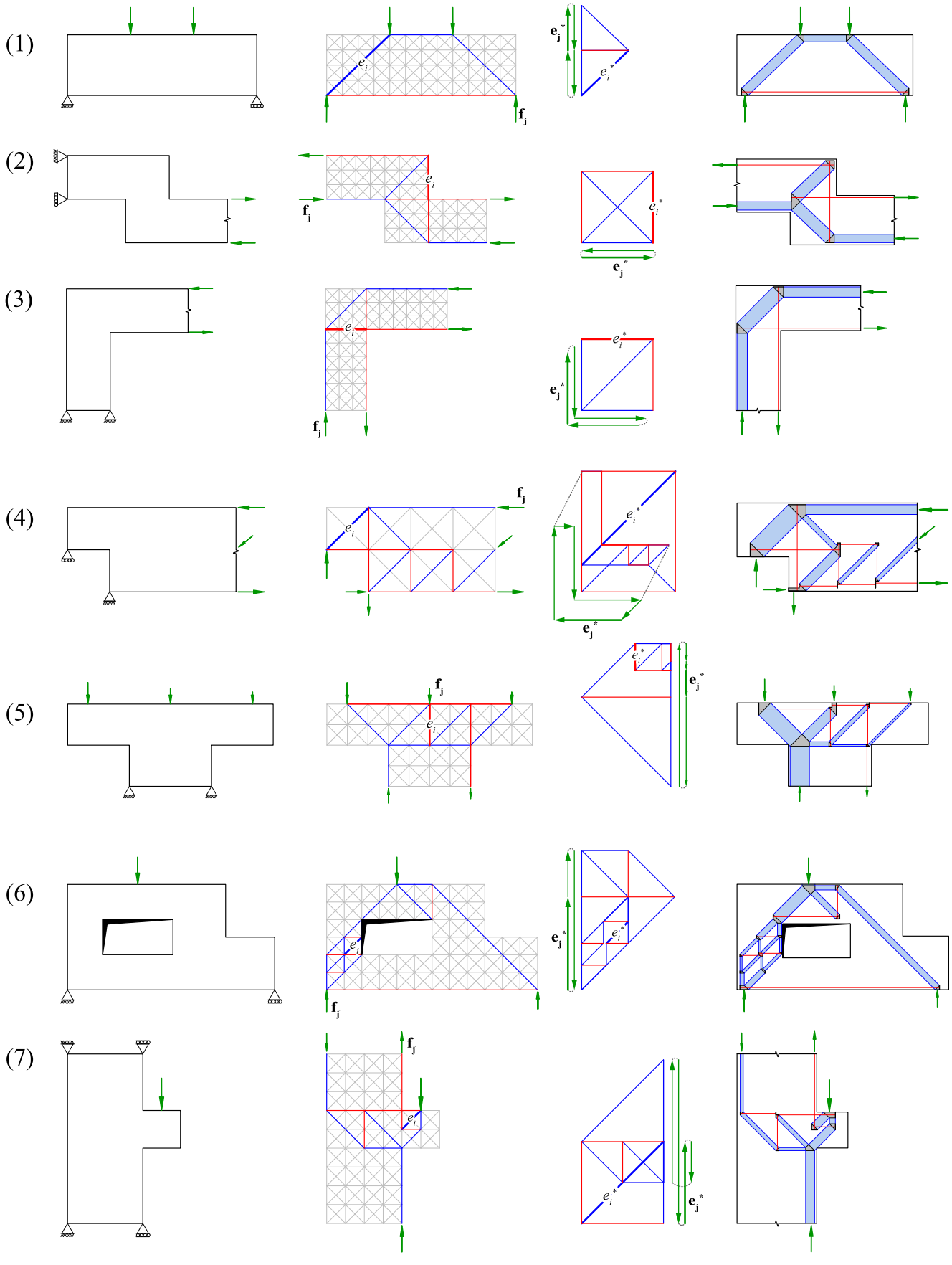

Fig. 9. (a) Input design domain and boundary conditions; (b) output form diagram (STM); (c) output force diagram; (d) output stress fields.

less than one second. All the algorithms are written in Python [63], where the algebraic implementations use NumPy and SciPy packages [64,65], the optimization is performed with the CVXPY package [66], which solves convex optimization problems. In our case, an interior-point method is used to solve the linear optimization problem. Also, the data structures such as meshes and graphs are created or modified using COMPAS [67].

3. Results

The previous section showed how the integrated algorithm automated the process of generating a valid truss model, its force diagram, and stress fields accounting for a continuous design domain under specified boundary conditions. It prevented the pre-definition of the form diagram and independent force densities of the indeterminate ground truss. These are typically required for

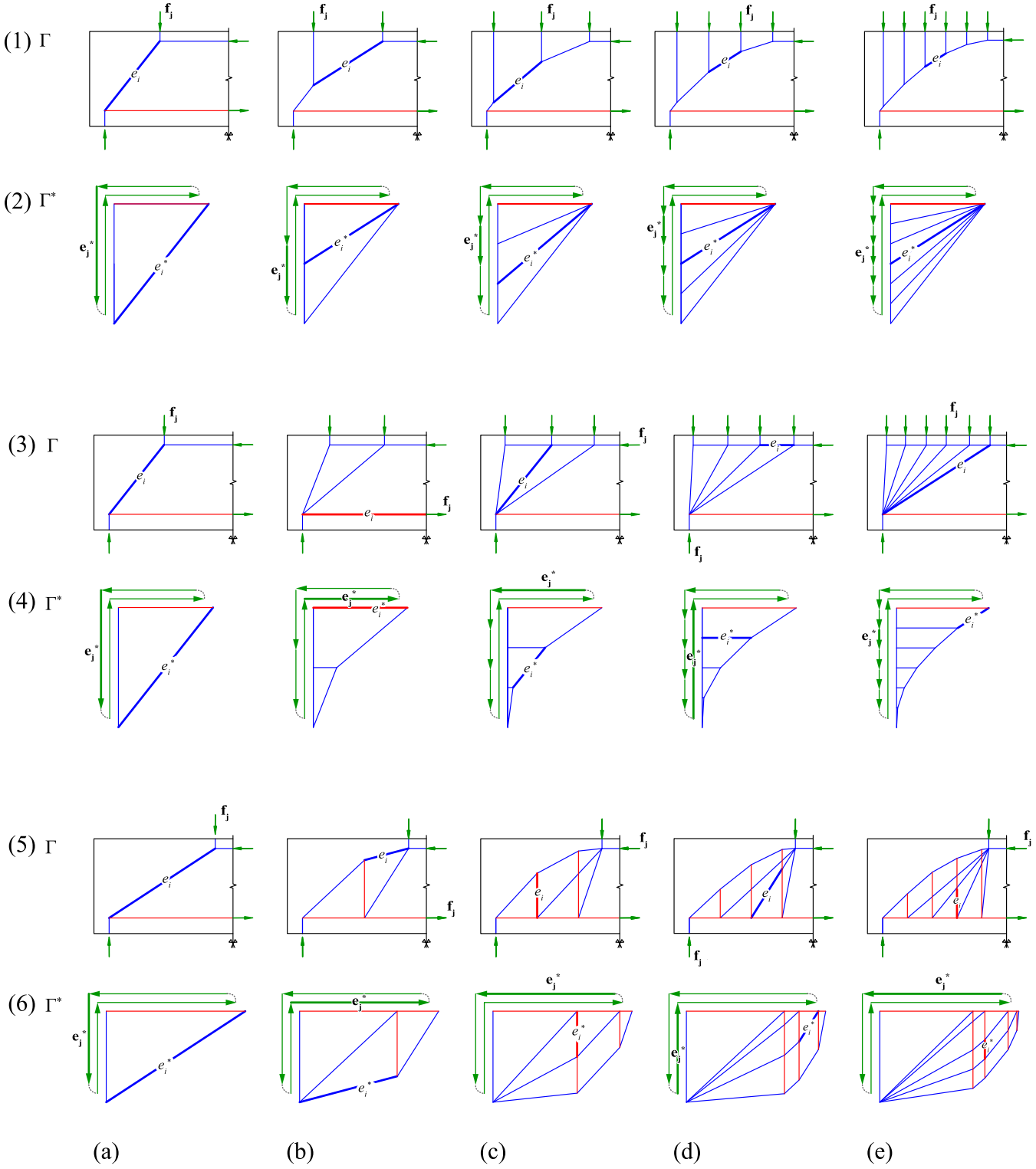

Fig. 10. Step-wise subdivision of external load through arching/funicular action(1a)-(1e) and fan-shaped behavior (3a)-(3e); (5a)-(5e) step-wise addition of stirrups (combination of the funicular and fan-shaped behavior); (2a)-(2e), (4a)-(4e), and (6a)-(6e) step-wise modifications of their corresponding force diagrams.

the production of the force diagram with the AGS formulation. The previous section also showed how, with the help of GS, one could modify the initial force diagram and reconstruct the form to produce a new strut-and-tie solution. Section 3.1 shows examples for the application of the integrated algorithm to several boundary conditions, and Section 3.2 provides examples for modification of the original form and force diagrams to generate new solutions.

3.1. Integrated algorithm

Fig. 9(1)-(7) shows the application of the integrated algorithm (i.e., Eqs. (4) and (5) along with the implementation of Minkowski sum) to a simply-supported beam, a stepped beam, a frame joint, a dapped-end beam, a hammerhead pier, a wall with an opening, and a corbel column. Other than initiating a valid STM, the method enables the visualization of forces through the force diagram and illustrates the concrete element's sufficiency to carry compression through constant stress fields.

3.2. Modifications with graphic statics

In order to modify the original solutions with the help of GS, proper procedures, such as adding reinforcement in specific directions/locations and subdivision of compression, tension, or external loads, could be adopted. The new strut-and-tie solutions can be reconstructed after the modifications of the force diagram, as explained in the example of Section 3.2. Fig. 10 shows a sample of the step-wise transformations that can be implemented to generate more elaborate STM solutions and their force diagrams while maintaining the static equilibrium.

The step-wise subdivision of the form and force diagrams in Fig. 10(1)-(4) illustrates the change from a point load in (a) to a distributed load in (e) for a simply-supported beam. The truss models in Fig. 10(1) and (3) are carrying the loads directly to the supports; the difference relies on the concrete's load transfer behavior, where in Fig. 10(1) an arching (funicular) and in Fig. 10(3) a fan-shaped action occurs. "Whether a fan or an arch mechanism occurs in a certain member depends, among other things, on the slenderness, the reinforcement ratio, and the loading history. In an elastic solution, the stiffest mechanisms will be formed" [57, 2.1: 12]. Considering that the funicular behavior uses a shorter load path and assuming that the model with the least load path has less deformation and therefore is stiffer, the STM in Fig. 10(1e) compare to Fig. 10(3e) is likelier to happen in the elastic range.

The other exciting modification is to transfer the load indirectly to the supports by adding stirrups, as in Fig. 10(5) and (6), where a

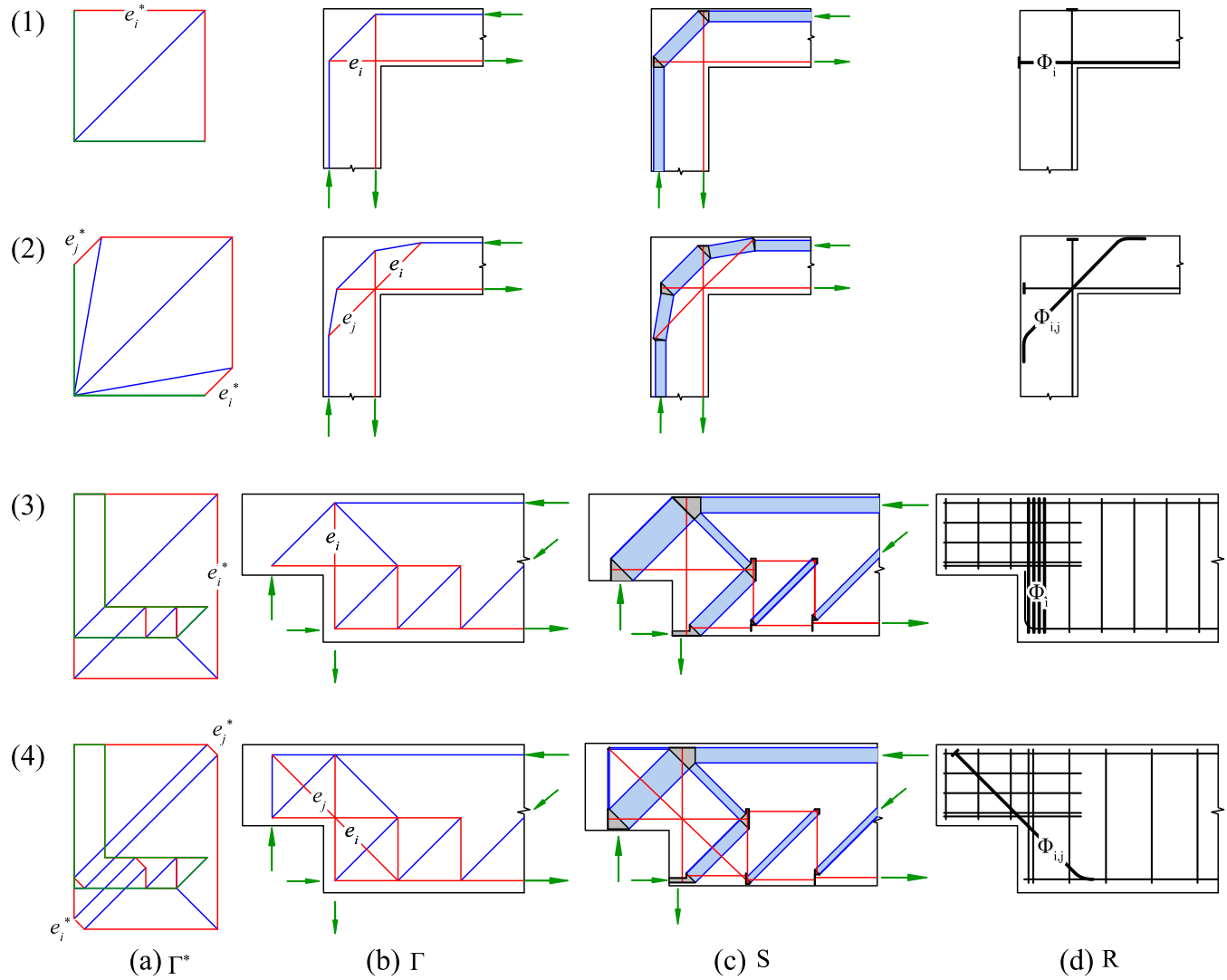

Fig. 11. (1a)-(1c) and (3a)-(3c) Original force diagrams, STMs, and stress fields from Fig. 9; (1d) and (3d) their schematic reinforcement designs; (2a)-(2c) and (4a)-(4c) modified force diagrams, STMs and stress fields with additional diagonal reinforcement; (2d) and (4d) their schematic reinfo.rcement designs.

combined funicular and fan-shaped behavior occurs. For example, in Fig. 10(5e), a portion of the external load transfers with the fan-shaped struts to the horizontal tie, then, passes through the stirrups to the arching struts on the top and eventually transfers along the other portion of the external load through the arch to the supports.

The next sections illustrate modification scenarios for the results in Fig. 9. The new force and form are available with the help of reciprocal relations, the equilibrium is satisfied, and the stress fields are reconstructed. In the following examples, the boundary conditions stay unchanged, and a schematic interpretation of the reinforcement layout is depicted. The location of ties, the magnitude of the tension forces, and fabrication rules help arrange the reinforcement for the given domain.

3.2.1. Diagonal reinforcement

Fig. 10(5) and (6) showed how adding the stirrups helps redistribute the tension force in the horizontal reinforcement. Now, using the outputs for the frame joint in Fig. 9(3) and dapped-end beam in Fig. 9(4), Fig. 11(2) and (4) demonstrate how a diagonal tie is added to the STM, where the forces, stress fields, and reinforcement arrangements are updated. Structural engineering practice uses diagonal reinforcements at specific locations such as cross-sectional changes or around openings. The diagonal bar helps the confinement of the region in avoiding cracks and improves the bending capacity of the concrete element [7, 62–67], [57, 2.1: 69–72].

Note that, although we constrained the diagonals to carry compression to get useful models in the optimization formulation, there was also a possibility to assign tension values to specific locations. However, the results will not be as clean, and the inclination of ties and struts is only restricted to 45-degree angles.

3.2.2. Subdivision of forces

Fig. 10 illustrated that the availability of the force and form diagrams allows the redistribution of tension and compression. Now, considering the output STMs for the frame joint in Fig. 9(3) and stepped beam Fig. 9(2), Fig. 12(2) and (4) show that the subdivision of the diagrams results in the force re-distributions in the discontinuity regions [7, 66–67]. The modified forces in Fig. 12(2a) and (4a) are half of the original forces in Fig. 12(1a) and (3a), which is also evident by looking at the stress fields in Fig. 12(2c) and (4c). The transformations created longer load paths, which could be assumed as a more plastic behavior compare to the original solutions (based on the earlier discussion).

3.2.3. Indeterminate cases

If the STM is indeterminate, e.g., Fig. 11(4b) and Fig. 12(2b), then manipulation of the force diagram, while the form stays unchanged, can create different force distributions, see Fig. 13(1a)-(1c) and (3a)-(3c). The reinforcement layout in Fig. 13(2d) and (4d) remains

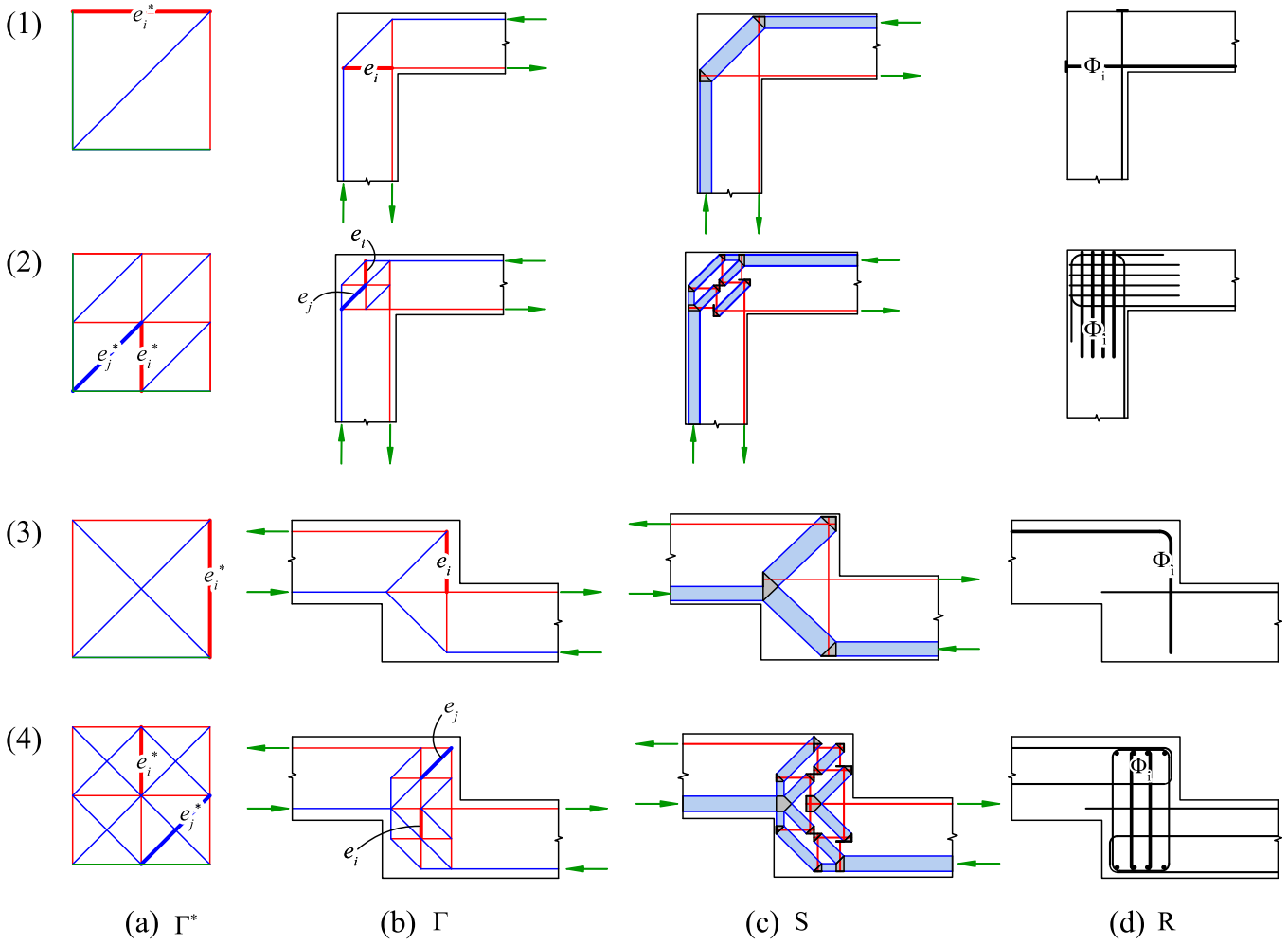

Fig. 12. (1a)-(1c) and (3a)-(3c) Original force diagrams, STMs, and stress fields from Fig. 9; (1d) and (3d) their schematic reinforcement designs; (2a)-(2c) and (4a)-(4c) modified force diagrams, STMs and stress fields with additional diagonal reinforcement; (2d) and (4d) their schematic reinfo.rcement designs.

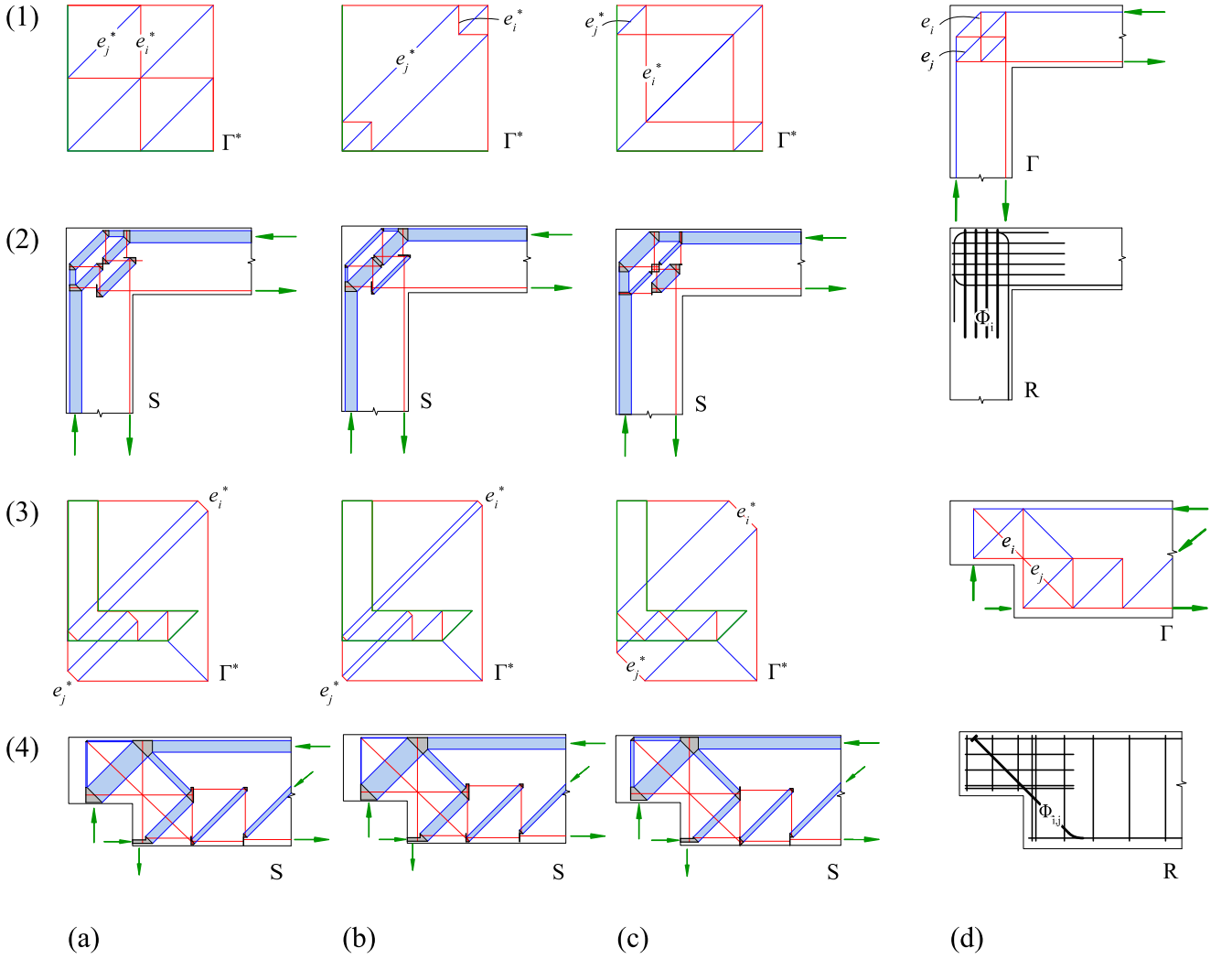

Fig. 13. (1a)-(1c) and (3a)-(3c) Variations of the force diagrams for the indeterminate STMs in (1d) and (3d); (2a)-(2c) and (4a)-(4c) their corresponding stress fields; (2d) and (4d) their schematic reinforcement designs (the size of reinforcement in Φ_i and $\Phi_{i,j}$ vary according to the amount of tension in e_i^* and e_j^*).

unchanged, if the size of the corresponding rebars, e.g., Φ_i, could get adjusted accordingly. The changes in the compression forces are apparent in the stress fields of Fig. 13(2a)-(2c), while they have not varied drastically in Fig. 13(4a)-(4c).

3.3. Evaluation

The STM solutions of a given problem can be evaluated or compared using an FEA-based stress field analysis software, such as IDEA StatiCa Detail [68]. As an example, the reinforcement patterns for the frame joint in Fig. 11(1d) and (2d) and Fig. 12(2d) are used as the rebar layouts in IDEA StatiCa Detail to carry out an evaluation.

Fig. 14(3) and (4) show the results of the stress analysis (*ultimate limit state*, ULS) and the crack width evaluation (*serviceability limit state*, SLS), given the boundary conditions, concrete cross-section, and reinforcement designs in Fig. 14(1) and (2). Each rebar has four layers along the 500 mm width of the cross-section. The least amount of reinforcement is used to satisfy the criteria for stress limitations, anchorage length, and crack widths.

Adding the diagonal reinforcement in Fig. 14(b) has reduced the crack widths utilization and the stresses in concrete and steel compare to the results of Fig. 14(a). Also, as expected, the compressive stresses in Fig. 14(3c) are distributed more evenly, i.e., have less concentration in comparison to Fig. 14(3a) and (3b). As a result, there is less utilization of concrete and reinforcement strength. However, using the reinforcement layout in Fig. 14(c) requires more steel and has larger crack widths compared to Fig. 14(b). The other observation could be that using the reinforcement design from the LAYOPT solution, i.e., Fig. 14(2a), with the minimized load path (or volume), does not necessarily provide the best engineering solution, and in this case, Fig. 14(2b) could be a more desirable design with reasonable use of material compared to the other two solutions.

4. Discussion and conclusions

This paper presented a methodology to bridge the gap between LAYOPT and GS by utilizing their advantages. Thus, the reliance on the single optimization solution as the only valid answer and the pre-definition of an initial diagram for GS were avoided. The developed algorithm embedded the algebraic formulation of GS for indeterminate trusses into the LAYOPT equations, then combined it with the Minkowski sum operation to produce a valid truss model, force diagram, and constant stress fields.

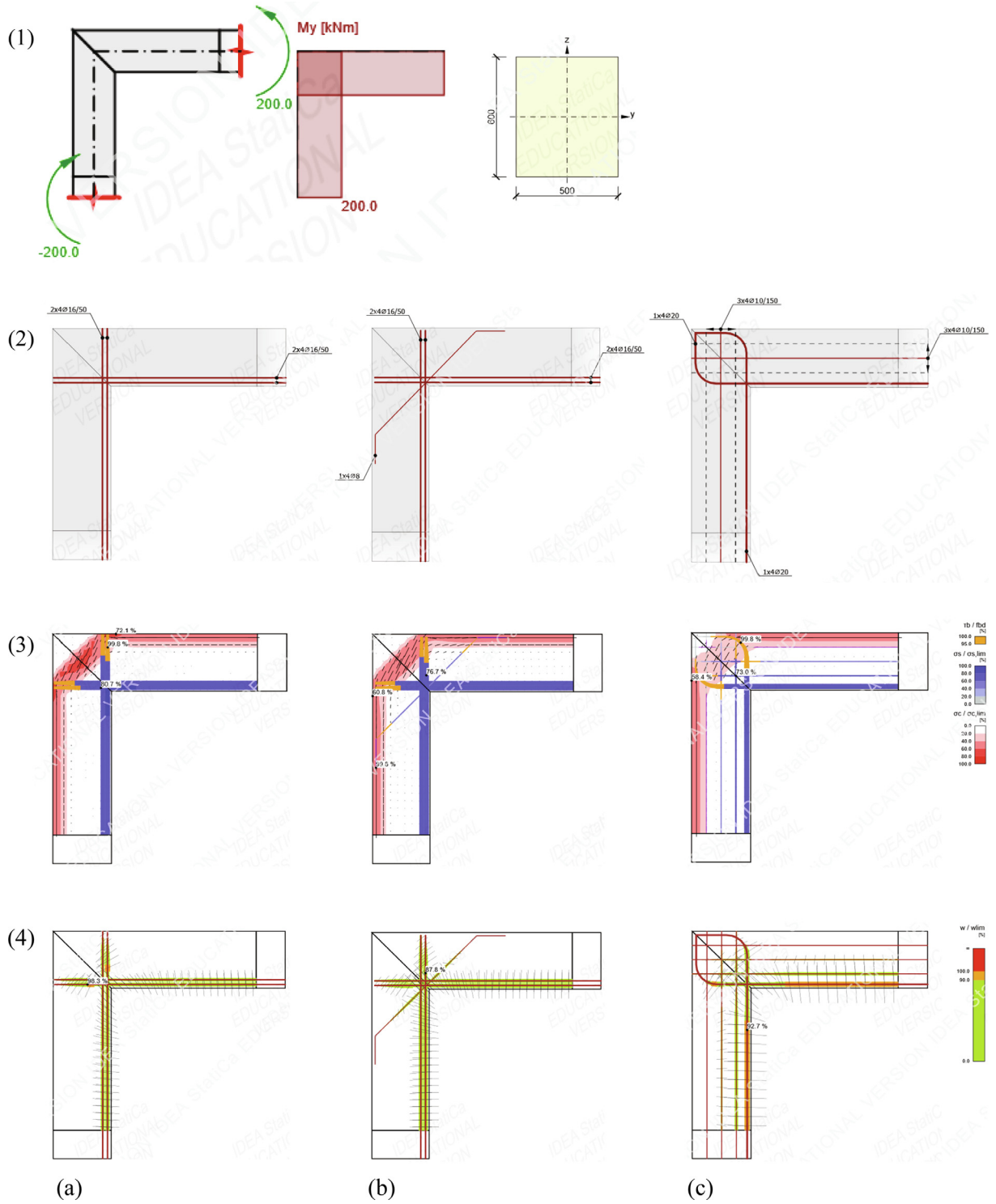

Fig. 14. (1) Boundary conditions and cross-sectional area (dimensions in mm) for the beam and column; (2) reinforcement designs; outputs of IDEA StatiCa Detail: (3) ULS, stress flow (blue: tension, red: compression, orange: stress in the anchorage, numbers show the utilization percentage of concrete, steel, and anchorage strength); (4) SLS, crack width check (numbers show the utilization percentage of the crack width).

The availability of the form and force diagrams allowed the modification of the initial diagrams and access to the updated internal forces, while the equilibrium was assured. As a result, a variety of STM solutions with constant stress fields and various reinforcement arrangements are produced. The utilization of GS provided a desirable level of control to systematically create practical STMs while helped in the understanding of their force distribution patterns. Furthermore, the generated results could provide better structural performances beyond the single optimization solution, aiming to minimize material usage. The performance evaluation of multiple reinforcement designs for a given problem was carried out using a stress field analysis software [68].

Aside from creating several designs, this paper provided a novel algorithm to automatically construct form and force diagrams in a continuum under given boundary conditions, where the complexities of the AGS method such as pre-defining the independent force

densities for the indeterminate ground truss, and the planarity requirement of the form diagram were avoided. Although the load path minimization objective was similar to [38,47], instead of a manually defined starting geometry for the truss, non-linear optimization equations, and nodal locations as optimization variables, the integrated algorithm used an automatically generated ground truss, the equations were linear, and the nodal locations were fixed. Although the fixed nodal locations in our case could cause longer load paths, the resulting geometries are practical and directly convertible to reinforcement designs. Similar to the solutions of topology optimization and layout optimization with full ground truss, e.g., Fig. 1, the tension paths in the solutions of [47] in many cases are not directly usable for reinforcement design. Another point is that the generated force diagrams in [47] are not easily readable, which poses a challenge in case of their utilization in a further step.

4.1. Limitations and future research

It is shown that the optimization results are affected by the geometry of the domain, mesh definition, connectivity of the nodes in the ground truss, and the optimization formulation. Therefore, for domains with irregular geometries or non-rectangular meshes, the user sometimes requires to investigate a variety of ground truss definitions or optimization constraints in order to have a valid initial model. Having cleaner initial results can facilitate the modifications and generation of other designs.

The examples presented here were limited to modifications that can produce other conventional STM solutions, however using GS also allows alternative and creative forms [42,45,46], where the validity of the STM and the reinforced concrete behavior is to be tested. Furthermore, the provided methodology applies to other materials such as reinforced masonry and timber connections, where strut-and-tie models and stress fields have been employed [69,70].

A significant amount of research on STM and stress fields has been conducted only in two-dimensional domains, and the authors are currently seeking to use the recent developments of three-dimensional GS [41,54,71] to generate a variety of three-dimensional truss models for reinforced concrete design.

Declaration of Competing Interest

The authors declare that they have no known competing financial interests or personal relationships that could have appeared to influence the work reported in this paper.

Acknowledgments

The authors would like to thank Dr. Tino Stankovic of Engineering Design and Computing Laboratory at ETH Zurich and Prof. Marton Hablicsek of Leiden University for their insightful support and constructive comments.

References

[1] Leondardt F. Reducing the shear reinforcement in reinforced concrete beams and slabs. Mag Concr Res 1965;17(53):187–98.
[2] Marti P. Basic tools of reinforced concrete beam design. ACI J 1985;82(4):46–56.
[3] Ritter W. The Hennebique construction method. Die Bauweise Hennebique, Schweizerische Bauzeitung 1899;33(7):41–61.
[4] Mörsch E. Der Eisenbetonbau, seine Theorie und Anwendung, volume 1. K. Wittwer, 1912..
[5] Drucker D. On structural concrete and the theorems of limit analysis. Int Assoc Bridge Struct Eng (IABSE)-Rep 1961;21:45–59.
[6] Nielsen MP, Braestrup MW, Jensen BC, Bach F. Concrete plasticity, beam shear–shear in joints–punching shear. In: Special Publication, Danish Society for Structural Science and Engineering; 1978. p. 1–129..
[7] Muttoni A, Schwartz J, Thürlimann B. Design of concrete structures with stress fields. Springer Science & Business Media; 1996.
[8] Schlaich J, Schäfer K, Jennewein M. Toward a consistent design of structural concrete. PCI J 1987;32(3):74–150.
[9] Schlaich J, Schäfer K. Design and detailing of structural concrete using strut-and-tie models. Struct Eng 1991;69(6):113–25.
[10] CSA. Canadian Standards Association: Design of concrete structures. Mississauga, Ontario, Canada; 2004..
[11] ACI 318. American Concrete Institute: Building code requirements for structural concrete (ACI 318-011); 2011..
[12] *fib* Model Code. CEB-FIP. International Federation for Structural Concrete (fib), Lausanne, Switzerland; 2010..
[13] Mitchell D, Collins MP. Revision of strut-and-tie provisions in the AASHTO LRFD bridge design specifications. Final Rep. for NCHRP 20-07/Task, 306; 2013..
[14] Muttoni A, Fernández Ruiz M, Niketic F. Design versus assessment of concrete structures using stress fields and strut-and-tie models. ACI Struct J 2015;112(S49).
[15] Meléndez C, Miguel PF, Pallarés L. A simplified approach for the ultimate limit state analysis of three-dimensional reinforced concrete elements. Eng Struct 2016;123:330–40.
[16] Liang QQ, Xie YM, Steven GP. Topology optimization of strut-and-tie models in reinforced concrete structures using an evolutionary procedure. ACI Struct J 2000;97(2):322–32.
[17] Kwak HG, Noh SH. Determination of strut-and-tie models using evolutionary structural optimization. Eng Struct 2006;28(10):1440–9.
[18] Bruggi M. Generating strut-and-tie patterns for reinforced concrete structures using topology optimization. Comput Struct 2009;87(23–24):1483–95.
[19] Victoria M, Querin OM, Martí P. Generation of strut-and-tie models by topology design using different material properties in tension and compression. Struct Multidiscipl Optim 2011;44(2):247–58.
[20] Ali MA, White RN. Automatic generation of truss model for optimal design of reinforced concrete structures. Struct J 2001;98(4):431–42.
[21] Amir O, Sigmund O. Reinforcement layout design for concrete structures based on continuum damage and truss topology optimization. Struct Multidiscip Optim 2013;47(2):157–74.
[22] Yang Y, Moen CD, Guest JK. Three-dimensional force flow paths and reinforcement design in concrete via stress-dependent truss-continuum topology optimization. J Eng Mech 2014;141(1):04014106.
[23] Aage N, Sigmund O, Amir O, Maier D, Søndergaard FA. Topopt plugin for rhino and grasshopper; 2013. URL https://www.grasshopper3d.com/group/topopt. [Accessed 30.01.2020]..
[24] Bruggi M. A numerical method to generate optimal load paths in plain and reinforced concrete structures. Comput Struct 2016;170:26–36.
[25] Gaynor AT, Guest JK, Moen CD. Reinforced concrete force visualization and design using bilinear truss-continuum topology optimization. J Struct Eng 2012;139(4):607–18.
[26] Yun YM, Ramirez JA. Strength of concrete struts in three-dimensional strut-tie models. J Struct Eng 2016;142(11):04016117.
[27] Bołbotowski K, Sokół T. New method of generating strut and tie models using truss topology optimization. In: Advances in Mechanics: Theoretical, Computational and Interdisciplinary Issues: Proceedings of the 3rd Polish Congress of Mechanics (PCM) and 21st International Conference on Computer Methods in Mechanics (CMM), Gdansk, Poland, 2015, CRC Press; 2016. p. 97..
[28] Kostic N. Topologie des champs de contraintes pour le dimensionnement des structures en beton arme. PhD thesis, EPFL; 2009..
[29] Fivet C, Zastavni D. A fully geometric approach for interactive constraint-based structural equilibrium design. Comput Aided Des 2015;61:42–57.
[30] Enrique L, Schwartz J. Load path network method: an equilibrium-based approach for the design and analysis of structures. Struct Eng Int 2017;27(2):292–9.
[31] Maxwell JC. On reciprocal figures and diagrams of forces. Philosoph Mag Ser 4 1864;27(182):250–61.
[32] Rankine WJM. Principle of the equilibrium of polyhedral frames. Philosoph Mag Ser 4 1864;4:27(180):92.
[33] Culmann K. Die Graphische Statik. Zürich: Verlag Meyer und Zeller; 1864.
[34] Cremona L. Graphical statics: two treatises on the graphical calculus and reciprocal figures in graphical statics. Translated by Thomas Hudson Beare. Oxford: Clarendon Press; 1890.
[35] Wolfe WS. Graphical analysis: a text book on graphic statics. New York: McGraw-Hill Book Co., Inc.; 1921.
[36] Allen E, Zalewski W. Form and forces: designing efficient, expressive structures. John Wiley & Sons; 2009.
[37] Van Mele T, Lachauer L, Rippmann M, Block P. Geometry-based Understanding of Structures. J Int Assoc Shell Spatial Struct 2012;53(174):285–95.
[38] Beghini LL, Carrion J, Beghini A, Mazurek A, Baker WF. Structural optimization using graphic statics. Struct Multidiscip Optim 2014;49(3):351–66.
[39] Akbarzadeh M, Mahnia M, Taherian R, Hedracrete Tabrizi AH. prefab, funicular, spatial concrete. In: DISCIPLINES & DISRUPTION: Projects Catalog of the 37th Annual Conference of the Association for Computer Aided Design in Architecture (ACADIA).
[40] Lee J, Mueller C, Fivet C. Automatic generation of diverse equilibrium structures through shape grammars and graphic statics. Int J Space Struct 2016;31(2–4):146–63.

[41] D'acunto P, Jasienski J, Ohlbrock P, Fivet C, Schwartz J, Zastavni D. Vector-based 3d graphic statics: A framework for the design of spatial structures based on the relation between form and forces. Int J Solids Struct 2019;167:58–70.
[42] Akbarzadeh M, Van Mele T, Block P. Compression-only form finding through finite subdivision of the force polygon. In: Proceedings of International Association for Shell and Spatial Structures (IASS) Symposium, vol. 16, 2014. p. 1–7..
[43] Akbarzadeh M, Van Mele T, Block P. Three-dimensional compression form finding through subdivision. In: Proceedings of the International Association for Shell and Spatial Structures (IASS) Symposium, vol. 21, 2015. p. 1–7..
[44] Nielsen T, Akbarzadeh M, Goltermann P. Addressing buckling of compression members using subdivision of force diagrams. In: Proceedings of the International Association for Shell and Spatial Structures (IASS) Symposium, Hamburg, Germany; 2017..
[45] Lee J, Van Mele T, Block P. Form-finding explorations through geometric transformations and modifications of force polyhedrons. In: Proceedings of the International Association for Shell and Spatial Structures (IASS) Symposium, Tokyo, Japan.
[46] Tabatabaie ghomi A, Bolhassani M, Nejur A, Akbarzadeh M. Effect of subdivision of force diagrams on the local buckling, load-path and material use of founded forms. In: Proceedings of the International Association for Shell and Spatial Structures (IASS) Symposium, "Creativity in Structural Design", Boston, USA, 2018..
[47] Alic V, Persson K. Generating initial reinforcement layouts using graphic statics. In: Proceedings of the International Association for Shell and Spatial Structures (IASS) Symposium, vol. 2018, 2018. p. 1–8..
[48] Zanni G, Pennock GR. A unified graphical approach to the static analysis of axially loaded structures. Mech Mach Theory 2009;44(12):2187–203.
[49] McRobie A. Maxwell and Rankine reciprocal diagrams via Minkowski sums for two-dimensional and three-dimensional trusses under load. Int J Space Struct 2016;31(2–4):203–16.
[50] Mozaffari S, Akbarzadeh M, Vogel T. Generation of strut-and-tie models and stress fields for structural concrete. In: Structures Congress 2019: Blast, Impact Loading, and Research and Education. p. 353–61.
[51] Konstantatou M, D'Acunto P, McRobie A, Schwartz J. Applications of graphic statics to analysis and design of reinforced concrete: Stress fields and yield lines. In: Proceedings of the International fib Symposium on Conceptual Design of Structures. p. 185–92.
[52] Van Mele T, Block P. Algebraic graph statics. Comput Aided Des 2014;53:104–16.
[53] Alic V, Åkesson D. Bi-directional algebraic graphic statics. Comput Aided Des 2017;93:26–37.
[54] Hablicsek M, Akbarzadeh M, Guo Y. Algebraic 3d graphic statics: Reciprocal constructions. Comput Aided Des 2019;108:30–41.
[55] Kirsch U. Structural optimization: fundamentals and applications. Springer Science & Business Media; 2012.
[56] Zegard T, Paulino GH. Grand–ground structure based topology optimization for arbitrary 2d domains using matlab. Struct Multidiscip Optim 2014;50 (5):861–82.
[57] Kaufmann W. Advanced structural concrete lecture notes, 2019. URL https://concrete.ethz.ch/en/asc/membrane-elements. [Accessed 30.01.2020]..
[58] Akbarzadeh M, Hablicsek M. Geometric degrees of freedom and non-conventional spatial structural forms. In: Design Modelling Symposium Berlin. Springer; 2019. p. 3–17.
[59] Moore EH. On the reciprocal of the general algebraic matrix. Bull Am Mathe Soc 1920;26:394–5.
[60] Penrose R. A generalized inverse for matrices. In: Mathematical proceedings of the Cambridge philosophical society, vol. 51(3), Cambridge University Press, 1955. p. 406–413..
[61] Skiena S. The algorithm design manual: Text, vol.1. Springer Science & Business Media; 1998.
[62] Mozaffari S. AGS-OPT: The integration of algebraic graphic statics and layout optimization, 2020. URL https://github.com/salmamzfr/AGS_OPT_2D. [Accessed 30.01.2020]..
[63] Python Software Foundation. Python Language Reference, version 3.7.3, 2019. URL https://www.python.org. [Accessed 30.01.2020]..
[64] Jones E, Oliphant T, Peterson P et al. SciPy: Open source scientific tools for Python, 2001. URL http://www.scipy.org/. [Accessed 30.01.2020]..
[65] Oliphant T. NumPy: A guide to NumPy. USA: Trelgol Publishing, 2006. URL http://www.numpy.org/. [Accessed 30.01.2020]..
[66] Diamond S, Boyd S. CVXPY: A Python-embedded modeling language for convex optimization. J Mach Learn Res 2016;17(83):1–5.
[67] Mele TV, many others. COMPAS: A framework for computational research in architecture and structures., 2017-2019. URL http://compas-dev.github.io/. [Accessed 30.01.2020]..
[68] IDEA StatiCa Detail. User Guide, version 9.1, 2018. URL https://www.ideastatica.com/concrete/. [Accessed 30.01.2020]..
[69] Foraboschi P, Vanin A. Non-linear static analysis of masonry buildings based on a strut-and-tie modeling. Soil Dyn Earthq Eng 2013;55:44–58.
[70] Shope MG. Strength characterization of wood to wood connections using stress field analysis Master's thesis. Massachusetts Institute of Technology; 2016.
[71] Lee J, Van Mele T, Block P. Disjointed force polyhedra. Comput Aided Des 2018;99:11–28.